Discovery of the richest pulsating ultra-massive white dwarf

Francisco C. De Gerónimo, 1 Murat Uzundag, 2 Alberto Rebassa-Mansergas, 3,4 Alex Brown, 3 Mukremin Kilic, 5 Alejandro H. Córsico, 1 Gracyn C. Jewett, 5 and Adam G. ${\rm Moss}^5$

¹ Instituto de Astrofísica de La Plata, CONICET-UNLP, La Plata, Argentina
 ² Institute of Astronomy, KU Leuven, Celestijnenlaan 200D, 3001, Leuven, Belgium
 ³ Departament de Física, Universitat Politècnica de Catalunya, c/Esteve Terrades 5, 08860 Castelldefels, Spain
 ⁴ Institut d'Estudis Espacials de Catalunya, Esteve Terradas, 1, Edifici RDIT, Campus PMT-UPC, 08860 Castelldefels, Barcelona, Spain
 ⁵ Homer L. Dodge Department of Physics and Astronomy, University of Oklahoma, 440 W. Brooks St., Norman, OK 73019, USA

ABSTRACT

The discovery of pulsations in ultra-massive white dwarfs can help to probe their interiors and unveil their core composition and crystallized mass fraction through asteroseismic techniques. To date, the richest pulsating ultra-massive white dwarf known is BPM 37093 with 8 modes detected, for which detailed asteroseismic analysis has been performed in the past. In this work, we report the discovery of 19 pulsation modes in the ultra-massive white dwarf star WD J0135+5722, making it the richest pulsating hydrogen-atmosphere ultramassive white dwarf known to date. This object exhibits multiperiodic luminosity variations with periods ranging from 137 to 1345 s, typical of pulsating white dwarfs in the ZZ Ceti instability strip, which is centered at $T_{\rm eff} \sim 12\,000$ K. We estimate the stellar mass of WD J0135+5722 by different methods, resulting in $M_{\star} \sim 1.12-1.14 M_{\odot}$ if the star's core is made of oxygen and neon, or $M_{\star} \sim 1.14-1.15 M_{\odot}$ if the star hosts a carbon oxygen core. Future analysis of the star periods could shed light on the core chemical composition through asteroseismology.

1. INTRODUCTION

ZZ Ceti stars are pulsating hydrogen (H)-rich atmosphere (DAV) white dwarfs (WDs) with effective temperatures in the range $10400 \text{K} \lesssim T_{\text{eff}} \lesssim 13000 \text{ K}$ and surface gravities from $\log g \sim 7.5$ to ~ 9.4 (Winget & Kepler 2008; Fontaine & Brassard 2008; Althous et al. 2010; Córsico et al. 2019a; Saumon et al. 2022; Kilic et al. 2023). These objects constitute the most common class of pulsating WDs with more than 500 members known to date (Bognar & Sodor 2016; Córsico et al. 2019a; Vincent et al. 2020; Guidry et al. 2021; Romero et al. 2022, 2024). The pulsations in these objects are multiperiodic, with periods in the range $100 \lesssim \Pi \lesssim 1500 \,\mathrm{s}$ and amplitudes ranging from 0.01 up to 0.3 magnitudes. The variations in brightness are due to non-radial g (gravity) modes with low harmonic degree ($\ell \leq 2$) and generally low to moderate radial order $(1 \leq k \leq 15)$, excited by the $\kappa - \gamma$ mechanism (Dolez & Vauclair 1981; Winget et al. 1982) and the convective-driving mechanism (Brickhill 1991; Goldreich & Wu 1999). The existence of the red (cool) edge of the ZZ Ceti instability strip can be explained in terms of excited modes suffering enhanced radiative damping that exceeds convective driving, rendering them damped (Luan & Goldreich 2018). In many cases, the ZZ Ceti pulsation spectrum exhibits rotational frequency splitting (Brickhill 1975), which allows constraints on the rotation period (e.g. Hermes et al. 2017).

Most WDs are found in the $0.5-1.05~M_{\odot}$ range, and those are expected to have carbon and oxygen (CO) cores (Althaus et al. 2010). Below $0.5~M_{\odot}$, low-mass WDs are expected to harbor He-cores (Norris 2004; Althaus et al. 2017). However, at the other extreme, the core composition of ultra-massive (UM) WDs $(M_{\rm WD}/M_{\odot} \gtrsim 1.05)$ is uncertain, as they could harbor CO, oxygen and neon (ONe) (Siess 2010; Althaus et al. 2021), or even hybrid CO-Ne cores (De Gerónimo et al. 2024).

From the light that the stars emit, we can learn about the characteristics of their surface layers. However, we can probe the interiors of those stars that show variations in their luminosity due to pulsation modes by means of asteroseismology. This technique compares pulsating stars' observed frequencies (periods) with those derived by appropriate theoretical models, allowing us to obtain details about their internal structure and evolution. The larger the number of frequencies detected in a given star, the better the asteroseismic analysis becomes. Until now, five pulsating UM DAV WDs with masses $M_{\rm WD}/M_{\odot} \gtrsim 1.1$ have been reported in the literature. Among them, BPM 37093 $(T_{\rm eff} = 11\,370~{\rm K},~\log g = 8.84,~{\rm Nitta}~{\rm et}~{\rm al.}~2016)$ is

the richest pulsating UM WD known so far, with eight pulsation modes detected (Metcalfe et al. 2004) and it has been the target of detailed asteroseismic analysis (Córsico et al. 2019b). The remaining objects are GD 518 ($T_{\rm eff}=12\,030$ K, $\log g=9.084$, Hermes et al. 2013), SDSS J084021.23+522217.4 ($T_{\rm eff}=12\,160$ K, $\log g=8.93$, Curd et al. 2017), WD J212402.03-600100.0 ($T_{\rm eff}=12\,510$ K, $\log g=8.98$, Gentile Fusillo et al. 2019) and WD J004917.14-252556.81 ($T_{\rm eff}=13\,020$ K, $\log g=9.34$, Kilic et al. 2023). These objects show, at most, three pulsations modes reported in the literature, preventing comprehensive asteroseismological analyses from being carried out.

We have begun a program aimed at increasing the number of detected UM DAVs and the pulsation modes in already known DAVs with the Gran Telescope Canarias (GTC) and Apache Point Observatory (APO). In this work, we report the discovery of pulsations in WD J0135+5722 ($T_{\text{eff}} = 12415 \text{ K}, \log g = 8.90, \text{ Jew-}$ ett et al. 2024; Kilic et al. 2024; Jiménez-Esteban et al. 2023). Since we detect an exceptionally high number (19) of pulsation periods, this star constitutes the richest pulsating UM WD known to date. The paper is organized as follows. In Sect. 2 we describe the methods applied to obtain the pulsation periods of the target star. In section 3 we derive the stellar mass and the percentage of crystallized core employing different methods. Specifically, we use surface gravity and effective temperature along with evolutionary tracks to derive the spectroscopic mass, and the Gaia parallax and magnitudes to derive the astrometric mass and the photometric mass. Finally, in Sect. 4, we summarize our results.

2. CANDIDATE SELECTION AND PHOTOMETRIC OBSERVATIONS

To identify UM WD candidates, we utilized the catalog provided by Jiménez-Esteban et al. (2023). Our selection criteria included objects with a declination greater than -10 degrees, a probability of being DA type greater than 0.5, and masses exceeding $1M_{\odot}$ (adjusted from $1.05M_{\odot}$ to account for potential errors). We selected objects that lie within the instability strip defined by Hollands et al. (2020), which is crucial for identifying potential pulsating UM WDs. This process resulted in a total of 19 candidates, including WD J0135+5722. We supplemented our list with additional ultra-massive DA white dwarfs near the instability strip from Jewett et al. (2024, see their Table 6), which includes $M > 0.9 M_{\odot}$ white dwarfs within 100 pc and the Pan-STARRS footprint. It is noteworthy that 14 of the selected UM WDs have been observed with TESS. However, no significant pulsational peaks were detected above the threshold,

which is not entirely unexpected given the faintness of these objects.

High-speed photometry was obtained on the night of 2024 Sep 17 with the HiPERCAM imager (Dhillon et al. 2021) mounted on the 10.4m GTC telescope in Data were taken simultaneously in the La Palma. Super-SDSS $u_s/g_s/r_s/i_s/z_s$ filters with exposure times of 10.3/2.1/4.1/4.1/4.1 seconds in each band, respectively, with 4x4 binning for a continuous 4h. HiPER-CAM uses frame-transfer CCDs so dead time between exposures is negligible. The HiPERCAM data reduction pipeline was used to debias, flat-field, and fringe subtract the frames before extracting differential photometry relative to a bright comparison star in the field to remove effects due to variations in observing conditions. A variable target aperture size, set to 1.0×FWHM was used to minimize any effects due to the seeing variation and maximize the signal-to-noise ratio of the extracted photometry.

Additionally, high-speed photometry of WD J0135+5722 on UT 2023 Dec 23 and 2024 Sep 1 was acquired by using the APO 3.5m telescope with the ARCTIC imager and the BG40 filter. Even though the APO observations are relatively short, they confirm multi-periodic oscillations in WD J0135+5722 over several nights. We obtained back-to-back exposures of 10 s over 92 min on December 23 and 62 min on September 1. To reduce read-out time, we binned the CCD by 3×3 , resulting in a plate scale of 0.34 arcsec pixel⁻¹. This setup has a read-out time of 4.5 s, which results in a cadence of 14.5 s in our light curves.

2.1. Light curve analysis

We used a two-step process to analyze the light curves obtained from the HiPERCAM and APO observations, focusing on enhancing the accuracy of the frequency analysis. First, we applied a 5- σ clipping method to identify and remove outliers from the data. This technique involves calculating the mean and standard deviation of the flux values and then eliminating data points that deviate significantly (more than 5 standard deviations) from the mean. Following the clipping process, we implemented a second-order polynomial detrending to remove long-term systematic variations that could obscure the underlying periodic signals in the light curves. This method involves fitting a polynomial curve to the clipped data and subtracting this fitted curve from the original data, thereby isolating the short-term fluctuations of interest. The final light curves are shown in Fig. 1 for HiPERCAM observations and Fig. 2 for APO observations.

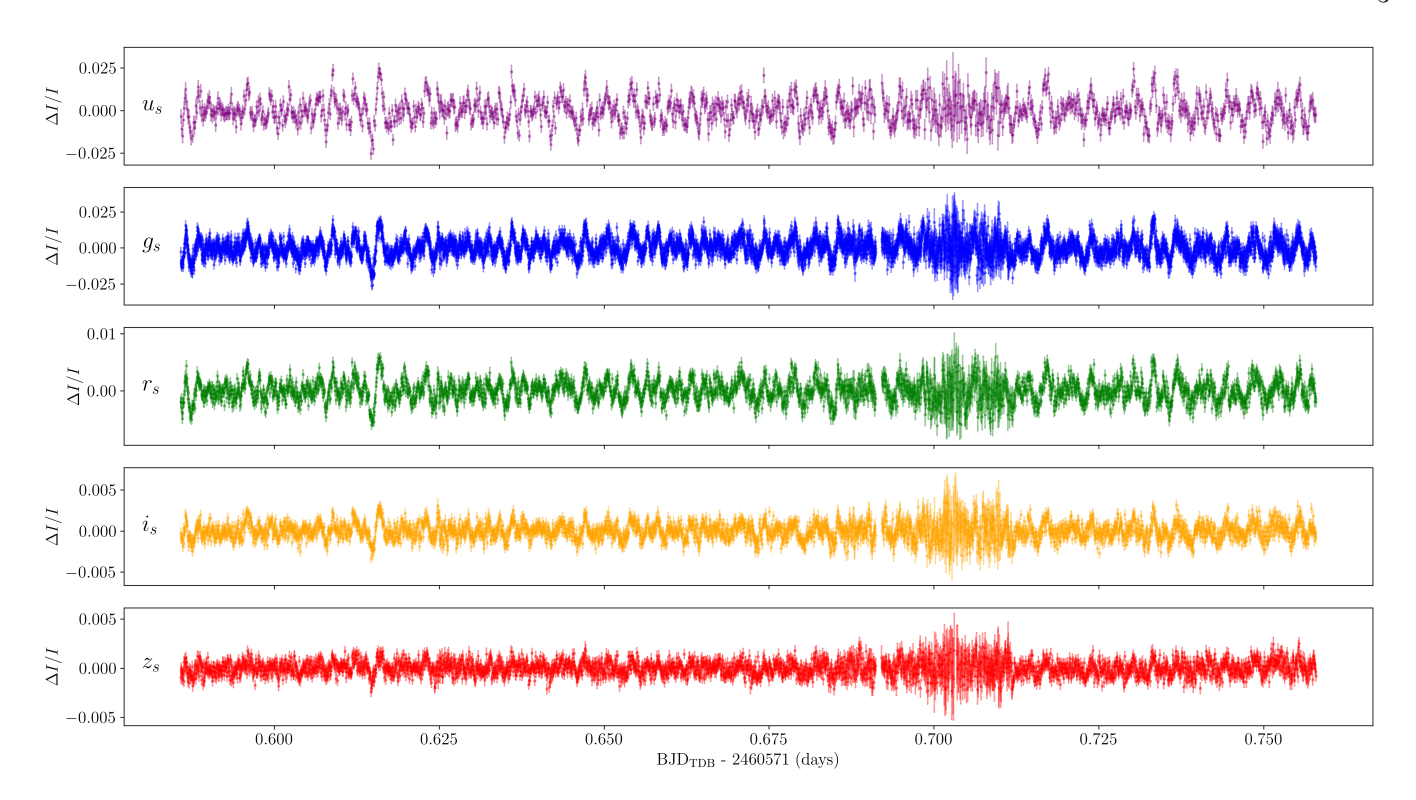


Figure 1. Light curve obtained with HiPERCAM on September 17 (see Sec. 2). HiPERCAM filters u_s, g_s, r_s, i_s, z_s are shown from top to bottom. The increased scatter at BJD 2460571.7 is due to an increase in the seeing and is unrelated to the target.

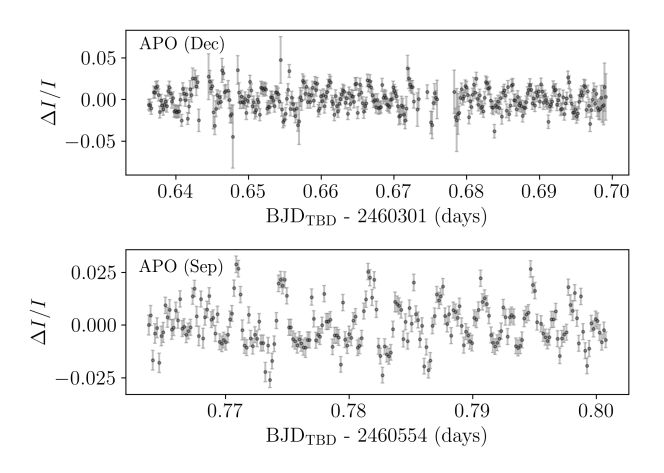


Figure 2. Light curve obtained with APO on December 23 (upper panel) and September 01 (bottom panel) (see Sec. 2 for more details).

2.2. Frequency analysis

To investigate the periodicities in the light curves of WD J0135+572, we computed the Fourier Transforms (FT) of each light curve. This analysis allows us to identify the frequencies of the star's pulsation modes, along with their respective amplitudes, phases and errors. The Fourier Transforms for the five bands of HiPERCAM are presented in Fig. 3, while Fig. 4 illustrates the FT from

APO data. For each Fourier amplitude spectrum, we computed the median noise level and established the detection threshold, represented by the dashed line in Fig. 3 for HiPERCAM and Fig 4 for APO, using an amplitude ratio of S/N > 4, as suggested by Breger et al. (1993); Sowicka et al. (2023). For all peaks exceeding this threshold within the frequency resolution of each dataset, we applied a non-linear least squares (NLLS) fit using the software Period04¹ (Lenz & Breger 2005). For some pulsation modes, WD J0135+572 displayed variations in amplitude, frequency, and/or phase during the observation period, which led to excess residuals in the FT after the process of pre-whitening. We carefully analyzed all frequencies with residuals exceeding the threshold post-prewhitening. When nearby frequencies were within the resolution range, we only fitted and pre-whitened the highest amplitude frequency to avoid confusion with spurious or closely spaced signals. We also calculated the spectral window of each light curve shown in the right panels of Fig. 3 for HiPERCAM and Fig. 4 for APO to assess and judge the presence of aliases, which helped us better distinguish between genuine pulsation frequencies and potential artifacts in the data. All pre-whitened frequencies for WD J0135+572

¹ http://www.period04.net/

including both HiPERCAM and APO are given in Table 2, showing frequencies (periods) and amplitudes with their corresponding uncertainties and the $\rm S/N$ ratio.

To conduct a comprehensive analysis of the full FT for each light curve, we first created a combined list from the FT solutions of each light curve. Based on the analysis of all bands $(g_s, r_s, u_s, z_s, i_s, \text{APO September}, \text{and APO December})$, several recurring signals are identified, indicating robust frequencies that are consistent across multiple datasets. We present a frequency solution for each subset, including five bands from HiPERCAM and two nights from APO, in Table 2, which contains all prewhitened frequencies for WD J0135+572 and provides frequencies (periods), amplitudes, associated uncertainties, and the S/N ratio.

To simplify the analysis, we divided the combined FT into three frequency segments, each providing critical insights into the pulsational characteristic of WD J0135+572. In the first segment, we examined frequencies up to 2500 μ Hz, and detected several lowamplitude frequencies. The highest peak is located at 77 μ Hz, with a signal-to-noise ratio (S/N) of 7.75. However, this frequency corresponds to 3.6 hours, matching the observing window, and was therefore excluded from the final list. Around 2141 μ Hz, we observe an unresolved peak present in four bands— g_s, r_s, z_s , and i_s —from observations by the HiPERCAM. This peak is most prominent in the g_s and r_s bands, spanning frequencies between 2128 μ Hz and 2182 μ Hz. From this group, the strongest peak identified is at 2128 μ Hz, with an S/N of 6.5. Seven peaks were detected in this segment, ranging from 77 μ Hz to 2128 μ Hz, with S/N values between 4.29 and 7.75.

In the second segment, we focused on between μHz and 8000 μ Hz. This range contains higher amplitude peaks, where the most prominent signals appear. Most of these peaks are visible across all HiPERCAM observation bands, while only three peaks were detected in the data from the APO, between 3468 μ Hz and 6348 μ Hz. Noteworthy peaks include those around 3846 and 3940 μ Hz, which might be aliases, but they have been retained for future observations to confirm their nature. An exciting feature is an unresolved, tooth-shaped peak near 4259 μ Hz, where we performed a single extraction. One of the highest peaks in the GTC data appears at 5144 μ Hz, with a nearby peak at 5185 μ Hz in the APO data, suggesting they may correspond to the same mode. Additionally, a cluster of peaks near 6330 μ Hz presents a challenge due to slight positional variations between the HiPERCAM and APO datasets. The peak at 6317 μ Hz shows excess residuals, which shift across bands but are likely related. Another peak at 6390 μ Hz, with

an S/N of 9.5, was extracted for analysis. Ultimately, the frequencies in this region, including those around 6317, 6335, and 6347 $\mu{\rm Hz},$ were retained to investigate whether they are part of rotational multiplets. In total, we identified 15 peaks between 2777 $\mu{\rm Hz}$ and 7259 $\mu{\rm Hz},$ with S/N values ranging from 5 to 33.

In the final segment, frequencies beyond 8000 μ Hz exhibit lower S/N values, typically ranging from 4 to 9. The absence of peaks in the z-band or APO September data for this frequency range limits our interpretation, but a few significant peaks were detected between about 12 400 and 18 761 μ Hz. The peak at 14 518 μ Hz has the highest S/N ratio of 9 and is present in almost all bands. The final two peaks, located around 18 000 and 18 761 μ Hz, are well-resolved only in the g_s, r_s, u_s , and i_s bands. The final list includes 5 significant frequencies from this region.

We searched for combination frequencies in each band and the APO data using the method described in Uzundag et al. (2023). Combination frequencies, arising from nonlinear interactions in the surface convection zone, are commonly detected in various pulsating white dwarf classes and provide valuable insights into the thermal response timescale of the convection zone (Montgomery 2005). For WD J0135+572, the FT is inconclusive for identifying all combination frequencies, but we identified two candidates at 12 406 μ Hz and 14 518 μ Hz. Given their typically low S/N ratios, confirming these peaks and detecting additional combinations requires a longer baseline. Future observations will be crucial to resolving all combination frequencies beyond 8000 μ Hz.

WD J0135+5722 presents a compelling challenge for a steroseismic analysis. Despite its rich pulsation spectrum, no clear frequency splitting patterns were detected, complicating the identification of triplets or quintuplets.

3. THE MASS OF WD J0135+5722

We estimate the mass of WD J0135+5722 employing different methods. On the one hand, we calculate the spectroscopic mass using the surface gravity and the effective temperature, together with evolutionary tracks corresponding to ultramassive WD models with different masses and core chemical compositions (ONe and CO). We have considered the possibility that WD J0135+5722 has a core of either ONe or CO because, while it is believed that WD cores in the mass range of WD J0135+5722 should be composed of ONe (Camisassa et al. 2019; Siess 2007), it is not currently ruled out that they could be made of CO (e.g., Althaus et al. 2021). In the case of ONe-core DA WD models, we employ an extension of the

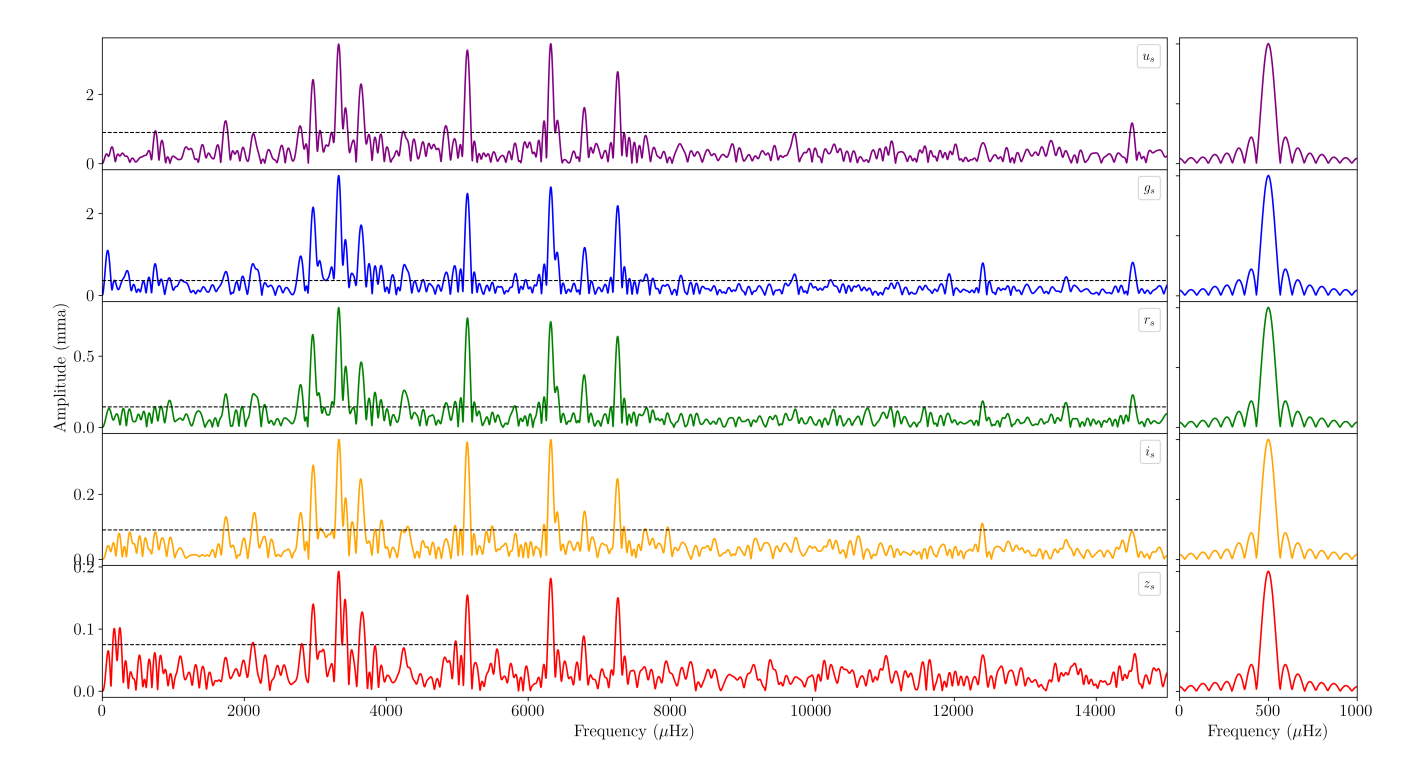


Figure 3. Fourier transform of the light curves obtained from HiPERCAM, with the same color scheme as in Fig. 1. The horizontal black dashed line indicates the significance level corresponding to S/N=4. The right panels display the spectral window for each light curve centered at 1000 μ Hz for a comparison.

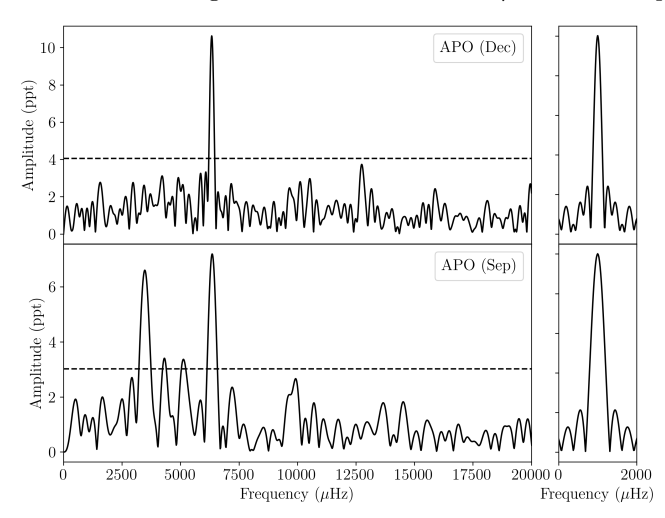


Figure 4. Fourier transform of the light curves obtained from APO on December 23 (upper panel) and on September 01 (bottom panel). The horizontal black dashed line indicates the significance level corresponding to S/N=4. The right panels display the spectral window for each light curve centered at 1000 μ Hz for a comparison.

model grid of Camisassa et al. (2019), which considers the progenitor's complete evolution in the super asymptotic giant branch. In particular, we consider a grid of model sequences with stellar masses of $M_{\rm WD}/M_{\odot}=$

1.10, 1.13, 1.16, 1.19, 1.23, 1.25, and 1.29 (De Gerónimo et al. 2025, in prep.). In the case of CO-core WD models, we consider the evolutionary tracks of Camisassa et al. (2022), which assume the same chemical profiles of C and O in the core for different values of the stellar mass $(M_{\rm WD}/M_{\odot} = 1.10, 1.16, 1.23, \text{ and } 1.29)$. All our models were generated with the LPCODE evolutionary code (Althaus et al. 2005) from the beginning of the WD's cooling track at high luminosities down to the development of the full Debye cooling at very low surface luminosities. Additionally, the correct assessment of crystallization and the release of energy due to phase separation are considered. The models of ONecore WDs of Camisassa et al. (2019) have been successfully employed in previous pulsational studies of H-rich UM WDs (see. e.g., De Gerónimo et al. 2019; Córsico et al. 2019b; Kilic et al. 2023).

In Fig. 5 we show the evolutionary tracks for our ONe- and CO-core WDs models in the $\log g-T_{\rm eff}$ plane and the spectroscopic determination of the effective temperature and surface gravity of for WD J0135+5722 from Jewett et al. (2024) ($T_{\rm eff}=12\,415\pm87$ K and $\log g=8.90\pm0.007$). The error in $\log g$ is taken from Kilic et al. (2020). In addition, we include the location of all the previously known pulsating UM ZZ Ceti stars, specifically BPM 37093 (Nitta et al. 2016), GD 518

(Hermes et al. 2013), SDSS J084021.23+522217.4 (Curd et al. 2017), WD J212402.03-600100.0 (Gentile Fusillo et al. 2019) and WD J004917.14-252556.81 (Kilic et al. 2023). From our evolutionary tracks, we found that, if the star under study harbors a ONe-core, it should have a mass of $1.118 \pm 0.002 M_{\odot}$. On the other hand, if a CO core composition is assumed we found the mass to be $1.135 \pm 0.004 M_{\odot}$, slightly lower than the $1.153 M_{\odot}$ predicted by Jewett et al. (2024), who employed CO-core evolutionary sequences from Bédard et al. (2020). According to our computations, this star would have a crystallized core of about 85.6 (56.0)% if a ONe(CO)-core composition is assumed.

The other methods we employed to obtain the stellar mass of WD J0135+5722 are based on astrometry and photometry. First, we calculated the astrometric mass (which uses Gaia distance and magnitudes together with atmospheric models and evolutionary tracks) and obtained $M_{\rm astr} = 1.137^{+0.004}_{-0.007} M_{\odot}$ (ONe-core WDs) and $M_{\rm astr} = 1.145^{+0.009}_{-0.001} M_{\odot}$ (CO-core WDs) full states of the content of the WDs) following the procedure of Calcaferro et al. (2024). In this method, distance versus effective temperature curves are calculated for different masses and the stellar mass of the target star is determined by interpolating the value of the Gaia distance of the star. To derive the photometric mass (see, e.g., Bergeron et al. 1997, 2001, 2019; Gentile Fusillo et al. 2019) we use the Gaia distance together with atmospheric models and mass-radius relations (see Calcaferro et al. 2024), resulting in $M_{\rm phot}=1.142^{+0.009}_{-0.008}M_{\odot}$ (ONe-core WDs) and $M_{\rm phot} = 1.153^{+0.010}_{-0.009} M_{\odot}$ (CO-core WDs). All stellar mass estimates (spectroscopic, astrometric, and photometric) for WD J0135+5722 are in excellent agreement. Table 1 summarizes all solutions derived from various techniques and models.

Regarding the H content of our ultramassive WD models, we have adopted the maximum expected to be $\sim 10^{-6} M_{\rm WD}$ for UM WDs. We have found that lower H-mass content could lead to differences in the mass determinations below $\sim 10^{-3} M_{\odot}$.

4. CONCLUSIONS AND FUTURE PROSPECTS

In this study, we report the discovery of pulsations in WD J0135+5722, a H-rich UM WD with $T_{\rm eff}=12\,415\pm87$ K and $\log g=8.90\pm0.007$. WD J0135+5722 displays an exceptionally high number of pulsation modes, surpassing any previously known UM WD. It presents a unique opportunity to investigate the interior of a potential ONe/CO-core WD using asteroseismic techniques.

Using the HiPERCAM and APO instruments, we identified 19 distinct pulsation periods, ranging from \sim 137 s (7259 μ Hz) to 1345 s (743 μ Hz), typical of ZZ

Table 1. Main parameters for WD J0135+5722.

~ .				
Parameters from Gaia				
412839403319209600				
01:35:17.57				
+57:22:49.29				
$\pi = 19.665^{+0.057}_{-0.057} \text{mas}$				
$d = 50.77^{+0.15}_{-0.13} \mathrm{pc}$				
16.668				
16.672				
16.712				
Parameters from spectroscopy				
12415 ± 87				
8.9 ± 0.007				
Parameters from evolutionary tracks				
1.118 ± 0.002				
0.85				
1.135 ± 0.004				
0.56				
Parameters from photometry and astrometry				
$1.137^{+0.004}_{-0.007}$				
$1.142^{+0.009}_{-0.008}$				
$1.145^{+0.009}_{-0.001}$				
$1.153^{+0.010}_{-0.009}$				

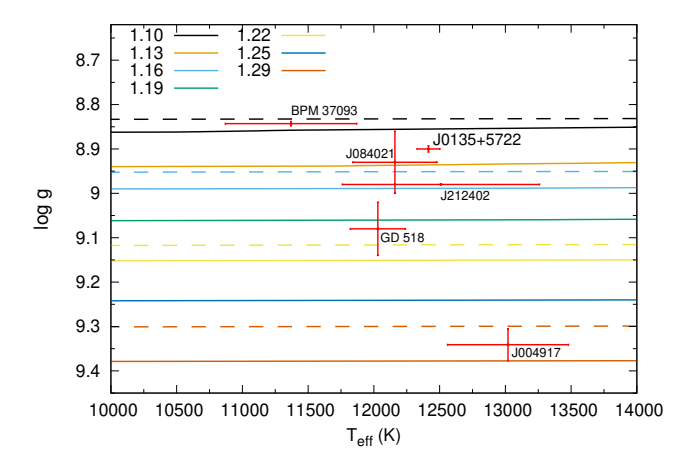


Figure 5. Location of our UM ONe(CO)-core WD evolutionary tracks, depicted with solid (dashed) lines, together with the determinations for WD J0135+5722 ($T_{\rm eff} = 12415 \pm 87$ K and $\log g = 8.9 \pm 0.007$) in the $\log g - T_{\rm eff}$ plane. We also include the spectroscopic determinations for the already known to pulsating UM WDs. The mass of WD J0135+5722 is $1.118 \pm 0.002 M_{\odot}$ if its core is made of ONe, and $1.135 \pm 0.0035 M_{\odot}$ if the star has a CO core.

Ceti stars. This is the sixth pulsating UM WD detected but the richest one in terms of the number of detected frequencies. This discovery is significant for future investigations, as it sheds light on the final stages of highmass stars and/or merger products, potentially serving as progenitors for supernovae.

WD J0135+5722 exhibits a complex picture for identifying pulsational modes, with overlapping modes, potential aliases, and deviations from expected patterns, making identifying through both period spacing and rotational splittings more difficult.

We derived a stellar mass of 1.118 or $1.135M_{\odot}$ if ONeor CO-core WD evolutionary sequences are adopted, with an 85 or 56% crystallized core, respectively. These masses are in excellent agreement with the astrometric and photometric masses derived employing the procedure from Calcaferro et al. (2024). UM WDs with masses in the range of masses of WD J0135+572 are likely to harbor an ONe-core (Camisassa et al. 2019; Siess 2007). However, different evolutionary channels suggest that some UM WD could have CO-cores (e.g., Althaus et al. 2021), or even hybrid CO-Ne cores (De Gerónimo et al. 2024). The question of whether this object harbors a core composed primarily of ¹²C and ¹⁶O or ¹⁶O and ²⁰Ne, could be answered by interpreting its pulsation spectrum. For instance, if enough pulsation g-modes of consecutive radial order are detected, a study of the forward period spacing could be employed to differentiate the core composition, given that noticeable differences exist in the period spacing between ONecore and CO-core models (De Gerónimo et al. 2019). On the other hand, the core chemical composition could be inferred by comparing the observed periods with theoretical periods computed on UM WD models. While a detailed set of UM WD models with ONe cores are already available (and have been successfully employed in several works, see De Gerónimo et al. 2019; Córsico

et al. 2019b; Kilic et al. 2023), to perform a robust and meaningful seismological analysis of WD J0135+5722, it is necessary also to consider UM WD models with CO cores. The computation of such a grid of models is currently in progress, and a detailed seismological analysis of WD J0135+5722 considering WD models with ONe and CO cores will be the focus of a future paper (De Gerónimo et al 2025, in prep.).

Based on observations made with the Gran Telescopio Canarias (Prog. ID: GTC19-24B), installed at the Spanish Observatorio del Roque de los Muchachos of the Instituto de Astrofísica de Canarias, on the island of La Palma. This work was supported by PIP 112-200801-00940 grant from CONICET, grant G149 from the University of La Plata, PIP-2971 from CON-ICET (Argentina) and by PICT 2020-03316 from Agencia I+D+i (Argentina). M. U. gratefully acknowledges funding from the Research Foundation Flanders (FWO) by means of a junior postdoctoral fellowship (grant agreement No. 1247624N). This work was partially supported by the MINECO grant PID2023-148661NB-I00 and by the AGAUR/Generalitat de Catalunya grant SGR-386/2021. This work is supported in part by the NSF under grant AST-2205736, the NASA under grants 80NSSC22K0479, 80NSSC24K0380, and 80NSSC24K0436. The Apache Point Observatory 3.5meter telescope is owned and operated by the Astrophysical Research Consortium.

This research has made use of the NASA Astrophysics Data System.

Facilities: Gran Telescopio Canarias (GTC), Apache Point Observatory (APO)

REFERENCES

Althaus, L. G., Córsico, A. H., Isern, J., & García-Berro, E. 2010, A&A Rv, 18, 471, doi: 10.1007/s00159-010-0033-1

Althaus, L. G., De Gerónimo, F., Córsico, A., Torres, S., & García-Berro, E. 2017, A&A, 597, A67, doi: 10.1051/0004-6361/201629909

Althaus, L. G., Serenelli, A. M., Panei, J. A., et al. 2005, A&A, 435, 631, doi: 10.1051/0004-6361:20041965

Althaus, L. G., Gil-Pons, P., Córsico, A. H., et al. 2021, A&A, 646, A30, doi: 10.1051/0004-6361/202038930

Bédard, A., Bergeron, P., Brassard, P., & Fontaine, G. 2020, ApJ, 901, 93, doi: 10.3847/1538-4357/abafbe

Bergeron, P., Dufour, P., Fontaine, G., et al. 2019, ApJ, 876, 67, doi: 10.3847/1538-4357/ab153a

Bergeron, P., Leggett, S. K., & Ruiz, M. T. 2001, ApJS, 133, 413, doi: 10.1086/320356

Bergeron, P., Ruiz, M. T., & Leggett, S. K. 1997, ApJS, 108, 339, doi: 10.1086/312955

Bognar, Z., & Sodor, A. 2016, Information Bulletin on Variable Stars, 6184, 1.

 $\rm https://arxiv.org/abs/1610.07470$

Breger, M., Stich, J., Garrido, R., et al. 1993, A&A, 271, 482

Brickhill, A. J. 1975, MNRAS, 170, 405, doi: 10.1093/mnras/170.2.405

—. 1991, MNRAS, 251, 673, doi: 10.1093/mnras/251.4.673
Calcaferro, L. M., Córsico, A. H., Uzundag, M., et al. 2024,
A&A, 691, A194, doi: 10.1051/0004-6361/202450582

- Camisassa, M. E., Althaus, L. G., Koester, D., et al. 2022, MNRAS, 511, 5198, doi: 10.1093/mnras/stac348
- Camisassa, M. E., Althaus, L. G., Córsico, A. H., et al. 2019, A&A, 625, A87, doi: 10.1051/0004-6361/201833822
- Córsico, A. H., Althaus, L. G., Miller Bertolami, M. M., & Kepler, S. O. 2019a, A&A Rv, 27, 7, doi: 10.1007/s00159-019-0118-4
- Córsico, A. H., De Gerónimo, F. C., Camisassa, M. E., & Althaus, L. G. 2019b, A&A, 632, A119, doi: 10.1051/0004-6361/201936698
- Curd, B., Gianninas, A., Bell, K. J., et al. 2017, MNRAS, 468, 239, doi: 10.1093/mnras/stx320
- De Gerónimo, F. C., Córsico, A. H., Althaus, L. G., Wachlin, F. C., & Camisassa, M. E. 2019, A&A, 621, A100, doi: 10.1051/0004-6361/201833789
- De Gerónimo, F. C., Miller Bertolami, M. M., Battich, T., et al. 2024, ApJ, 975, 259, doi: 10.3847/1538-4357/ad7d8e
- Dhillon, V. S., Bezawada, N., Black, M., et al. 2021, MNRAS, 507, 350, doi: 10.1093/mnras/stab2130
- Dolez, N., & Vauclair, G. 1981, A&A, 102, 375
- Fontaine, G., & Brassard, P. 2008, PASP, 120, 1043, doi: 10.1086/592788
- Gentile Fusillo, N. P., Tremblay, P.-E., Gänsicke, B. T., et al. 2019, MNRAS, 482, 4570, doi: 10.1093/mnras/sty3016
- Goldreich, P., & Wu, Y. 1999, ApJ, 511, 904, doi: 10.1086/306705
- Guidry, J. A., Vanderbosch, Z. P., Hermes, J. J., et al. 2021, ApJ, 912, 125, doi: 10.3847/1538-4357/abee68
- Hermes, J. J., Kepler, S. O., Castanheira, B. G., et al. 2013, ApJL, 771, L2, doi: 10.1088/2041-8205/771/1/L2
- Hermes, J. J., Gänsicke, B. T., Kawaler, S. D., et al. 2017, ApJS, 232, 23, doi: 10.3847/1538-4365/aa8bb5
- Hollands, M. A., Tremblay, P. E., Gänsicke, B. T., et al. 2020, Nature Astronomy, 4, 663, doi: 10.1038/s41550-020-1028-0
- Jewett, G., Kilic, M., Bergeron, P., et al. 2024, ApJ, 974, 12, doi: 10.3847/1538-4357/ad6905

- Jiménez-Esteban, F. M., Torres, S., Rebassa-Mansergas, A., et al. 2023, MNRAS, 518, 5106, doi: 10.1093/mnras/stac3382
- Kilic, M., Bergeron, P., Blouin, S., et al. 2024, arXiv e-prints, arXiv:2412.04611, doi: 10.48550/arXiv.2412.04611
- Kilic, M., Bergeron, P., Kosakowski, A., et al. 2020, ApJ, 898, 84, doi: 10.3847/1538-4357/ab9b8d
- Kilic, M., Córsico, A. H., Moss, A. G., et al. 2023, MNRAS, 522, 2181, doi: 10.1093/mnras/stad1113
- Lenz, P., & Breger, M. 2005, Communications in Asteroseismology, 146, 53, doi: 10.1553/cia146s53
- Luan, J., & Goldreich, P. 2018, ApJ, 863, 82, doi: 10.3847/1538-4357/aad0f4
- Metcalfe, T. S., Montgomery, M. H., & Kanaan, A. 2004, ApJL, 605, L133, doi: 10.1086/420884
- Montgomery, M. H. 2005, ApJ, 633, 1142, doi: 10.1086/466511
- Nitta, A., Kepler, S. O., Chené, A.-N., et al. 2016, IAU Focus Meeting, 29B, 493, doi: 10.1017/S1743921316005962
- Norris, J. E. 2004, ApJL, 612, L25, doi: 10.1086/423986
- Romero, A. D., Kepler, S. O., Oliveira da Rosa, G., & Hermes, J. J. 2024, arXiv e-prints, arXiv:2407.07260, doi: 10.48550/arXiv.2407.07260
- Romero, A. D., Kepler, S. O., Hermes, J. J., et al. 2022, MNRAS, 511, 1574, doi: 10.1093/mnras/stac093
- Saumon, D., Blouin, S., & Tremblay, P.-E. 2022, PhR, 988, 1, doi: 10.1016/j.physrep.2022.09.001
- Siess, L. 2007, A&A, 476, 893, doi: 10.1051/0004-6361:20078132
- —. 2010, A&A, 512, A10,doi: 10.1051/0004-6361/200913556
- Sowicka, P., Handler, G., Jones, D., et al. 2023, ApJS, 269, 32, doi: 10.3847/1538-4365/acfbe4
- Uzundag, M., De Gerónimo, F. C., Córsico, A. H., et al. 2023, MNRAS, 526, 2846, doi: 10.1093/mnras/stad2776
- Vincent, O., Bergeron, P., & Lafrenière, D. 2020, AJ, 160, 252, doi: 10.3847/1538-3881/abbe20
- Winget, D. E., & Kepler, S. O. 2008, ARA&A, 46, 157, doi: 10.1146/annurev.astro.46.060407.145250
- Winget, D. E., van Horn, H. M., Tassoul, M., et al. 1982, ApJL, 252, L65, doi: 10.1086/183721

APPENDIX

A. APPENDIX

Table 2. Frequency solution for WD J0135+5722.

ν	П	A	S/N
$(\mu { m Hz})$	(s)	(ppt)	5/11
	**		
743.0567 ± 4.183	Overall frequency s		7.01
951.5402 ± 5.5773	1345.7924 ± 7.5337 1050.9277 ± 6.1239	$0.7122 \pm 0.0801 \\ 0.2021 \pm 0.0312$	$7.91 \\ 5.63$
951.5402 ± 5.5775 1748.4132 ± 5.3341	571.9472 ± 1.7396	0.2021 ± 0.0312 0.1342 ± 0.0193	5.83
2128.3026 ± 1.1894	469.858 ± 0.2624	0.1342 ± 0.0193 0.8111 ± 0.0801	9.01
2777.2163 ± 3.7451	360.0728 ± 0.4849	0.7967 ± 0.0801	8.85
3331.9871 ± 0.9956	300.1212 ± 0.0896	2.9866 ± 0.0801	33.18
3416.0433 ± 3.1816	292.7363 ± 0.2724	0.9221 ± 0.0801	10.25
3468.4166 ± 16.0764	288.316 ± 1.3302	6.9527 ± 0.6478	9.22
3644.6761 ± 1.5346	274.3728 ± 0.1155	1.9304 ± 0.0801	21.45
3846.509 ± 5.6815	259.976 ± 0.3834	0.2057 ± 0.0314	5.73
3937.1916 ± 3.8922	253.9881 ± 0.2508	0.7529 ± 0.0801	8.37
3940.6543 ± 6.0918	253.765 ± 0.3917	0.1175 ± 0.0193	5.11
4259.9674 ± 6.0764	234.7436 ± 0.3344	1.2557 ± 0.0801	13.95
4840.4147 ± 6.041	206.5939 ± 0.2575	1.1995 ± 0.1925	5.33
5144.2384 ± 1.2187	194.3922 ± 0.046	2.4369 ± 0.0801	27.08
5185.0531 ± 27.7865	192.8621 ± 1.028	4.0226 ± 0.6478	5.33
6317.6627 ± 1.1259	158.2864 ± 0.0282	2.5794 ± 0.0801	28.66
6795.1019 ± 2.4933	147.1648 ± 0.054	1.1471 ± 0.0801	12.75
7259.092 ± 1.3482	137.7583 ± 0.0256	2.1881 ± 0.0801	24.31
	<i>u</i> -band		
1739.051 ± 5.8416	575.0263 ± 1.9251	1.2181 ± 0.1888	5.41
2768.3539 ± 6.9554	361.2255 ± 0.9053	0.9972 ± 0.1908	4.43
2966.8143 ± 2.9579	337.0619 ± 0.3357	2.436 ± 0.1912	10.83
3330.0977 ± 2.2832	300.2915 ± 0.2057	3.5388 ± 0.1947	15.73
3420.9185 ± 6.6355	292.3192 ± 0.5659	1.1771 ± 0.1951	5.23
3642.925 ± 2.8911	274.5047 ± 0.2177	2.4712 ± 0.1912	10.98
4840.4147 ± 6.041	206.5939 ± 0.2575	1.1995 ± 0.1925	5.33
5143.1508 ± 15.0907	194.4333 ± 0.5688	1.6413 ± 1.8991	7.29
6317.0944 ± 2.0431	158.3006 ± 0.0512	3.4252 ± 0.1903	15.22
6791.381 ± 4.2923	147.2455 ± 0.093	1.6115 ± 0.1906	7.16
7258.9402 ± 2.6556	137.7612 ± 0.0504	2.6392 ± 0.1903	11.73
14507.7891 ± 6.0182	68.9285 ± 0.0286	1.1632 ± 0.1894	5.17
	q-band		
743.0567 ± 4.183	1345.7924 ± 7.5337	0.7122 ± 0.0801	7.91
2128.3026 ± 1.1894	469.8580 ± 0.2624	0.8111 ± 0.0801	9.01
2182.0985 ± 1.2464	458.2745 ± 0.2616	0.6763 ± 0.0801	7.51
2777.2163 ± 3.7451	360.0728 ± 0.4849	0.7967 ± 0.0801	8.85
2972.2266 ± 1.3874	336.4481 ± 0.157	2.1541 ± 0.0801	23.93
3331.9871 ± 0.9956	300.1212 ± 0.0896	2.9866 ± 0.0801	33.18
3416.0433 ± 3.1816	292.7363 ± 0.2724	0.9221 ± 0.0801	10.25
3644.6761 ± 1.5346	274.3728 ± 0.1155	1.9304 ± 0.0801	21.45
3937.1916 ± 3.8922	253.9881 ± 0.2508	0.7529 ± 0.0801	8.37
4259.9674 ± 6.0764	234.7436 ± 0.3344	1.2557 ± 0.0801	13.95
5144.2384 ± 1.2187	194.3922 ± 0.046	2.4369 ± 0.0801	27.08
6317.6627 ± 1.1259	158.2864 ± 0.0282	2.5794 ± 0.0801	28.66
6388.2699 ± 3.0754	156.5369 ± 0.0753	0.8525 ± 0.0801	9.47
6795.1019 ± 2.4933	147.1648 ± 0.054	1.1471 ± 0.0801	12.75
7259.092 ± 1.3482	137.7583 ± 0.0256	2.1881 ± 0.0801	24.31
12406.6927 ± 3.898	80.6017 ± 0.0253	0.7596 ± 0.0801	8.44
14518.184 ± 3.665	68.8791 ± 0.0174	0.809 ± 0.0801	8.99
18001.4722 ± 4.6428	55.551 ± 0.0143	0.6392 ± 0.0801	7.10
18761.3401 ± 4.1854	53.3011 ± 0.0119	0.7093 ± 0.0801	7.88

Table 1. Frequency solution for WD J0135+5722 (continued).

u	П	A	S/N		
$(\mu { m Hz})$	(s)	(ppt)			
	,, band				
051 5400 5 5550	r-band	0.0001 0.0010	F (1)		
951.5402 ± 5.5773	1050.9277 ± 6.1239	0.2021 ± 0.0312	5.63		
1745.0508 ± 4.7649	573.0492 ± 1.5605	0.2430 ± 0.0310	6.77		
2135.0815 ± 4.5913	468.3662 ± 1.0050	0.2513 ± 0.0311	7.00		
2773.9248 ± 4.7151	360.5000 ± 0.6117	0.2452 ± 0.0315	6.83		
2965.5777 ± 1.8349	337.2024 ± 0.2085	0.6488 ± 0.0316	18.07		
3332.0720 ± 1.6993	300.1136 ± 0.1530	0.8470 ± 0.0321	23.59		
3422.8550 ± 5.1505	292.1538 ± 0.4390	0.2762 ± 0.0321	7.69		
3644.7690 ± 2.2869	274.3658 ± 0.1720	0.5217 ± 0.0315	14.53		
3846.5090 ± 5.6815	259.9760 ± 0.3834	0.2057 ± 0.0314	5.73		
4273.5253 ± 4.8581	233.9988 ± 0.2657	0.2390 ± 0.0312	6.66		
5144.3695 ± 1.5336	194.3873 ± 0.0579	0.7558 ± 0.0311	21.05		
6317.8238 ± 2.5577	158.2824 ± 0.0641	0.7294 ± 0.0416	20.32		
6385.0704 ± 6.7322	156.6153 ± 0.1650	0.2462 ± 0.0415	6.86		
6788.5504 ± 3.1643	147.3069 ± 0.0686	0.3584 ± 0.0313	9.98		
7259.2770 ± 1.8073	137.7548 ± 0.0343	0.6339 ± 0.0312	17.66		
14515.1917 ± 4.7955	68.8933 ± 0.0228	0.2384 ± 0.0310	6.64		
17991.8441 ± 5.7470	55.5807 ± 0.0177	0.1996 ± 0.0310	5.56		
17331.0441 ± 0.1410	00.0001 ± 0.0111	0.1330 ± 0.0310	0.00		
	i-band				
1748.4132 ± 5.3341	571.9472 ± 1.7396	0.1342 ± 0.0193	5.83		
2141.8061 ± 4.7928	466.8957 ± 1.0425	0.1493 ± 0.0193	6.49		
2784.0118 ± 6.0437	359.1939 ± 0.7781	0.1184 ± 0.0193	5.15		
2972.3024 ± 2.5243	336.4395 ± 0.2855	0.2836 ± 0.0193	12.33		
3335.4344 ± 1.9014	299.8110 ± 0.1708	0.3765 ± 0.0193	16.37		
3422.8550 ± 5.4009	292.1538 ± 0.4603	0.1325 ± 0.0193	5.76		
3641.4067 ± 2.6571	274.6191 ± 0.2002	0.2694 ± 0.0193	11.71		
3940.6543 ± 6.0918	253.7650 ± 0.3917	0.1175 ± 0.0193	5.11		
4300.4239 ± 7.1133	232.5352 ± 0.3840	0.1006 ± 0.0193	4.37		
5141.0072 ± 2.0002	194.5144 ± 0.0756	0.3579 ± 0.0193	15.56		
6317.8238 ± 1.9976	158.2824 ± 0.0500	0.3573 ± 0.0193 0.3583 ± 0.0193	15.58		
6391.7951 ± 6.4168	156.4506 ± 0.1569	0.3333 ± 0.0193 0.1115 ± 0.0193	4.85		
6795.2751 ± 4.8748	147.1611 ± 0.1055	0.1113 ± 0.0193 0.1468 ± 0.0193			
7255.9147 ± 2.8533	147.1011 ± 0.1035 137.8186 ± 0.0542		6.38		
		0.2509 ± 0.0193	10.91		
12396.9219 ± 6.5691	80.6652 ± 0.0427	0.1090 ± 0.0193	4.74		
18758.4560 ± 5.9698	53.3093 ± 0.0170	0.1199 ± 0.0193	5.21		
	z-band				
2972.3024 ± 4.2728	336.4395 ± 0.4829	0.1393 ± 0.0161	7.33		
3328.7097 ± 4.0058	300.4167 ± 0.3611	0.1849 ± 0.0168	9.73		
3416.1304 ± 5.7555	292.7289 ± 0.4924	0.1237 ± 0.0168	6.51		
3654.8560 ± 4.2284	273.6086 ± 0.3162	0.1362 ± 0.0162	7.17		
5034.3695 ± 3.9917	194.3873 ± 0.1507	0.1302 ± 0.0102 0.1491 ± 0.0160	7.85		
6317.8238 ± 3.2800	158.2824 ± 0.0821	0.1491 ± 0.0100 0.1803 ± 0.0161	9.49		
6781.8257 ± 6.7705	138.2824 ± 0.0821 147.4529 ± 0.1471	0.1803 ± 0.0161 0.0868 ± 0.0161	9.49 4.57		
	147.4529 ± 0.1471 137.6910 ± 0.0763				
7262.6394 ± 4.0242	191.0910 ± 0.0103	0.1469 ± 0.0161	7.73		
APO (23 December 2023)					
6335.8604 ± 8.2484	157.8318 ± 0.2052	10.5331 ± 0.8557	10.39		
-	DO (01 G : -				
	APO (01 September	,			
3468.4166 ± 16.0764	288.3160 ± 1.3302	6.9527 ± 0.6478	9.22		
5185.0531 ± 27.7865	192.8621 ± 1.0280	4.0226 ± 0.6478	5.33		
6347.5099 ± 14.8682	157.5421 ± 0.3682	7.5177 ± 0.6478	9.97		